Available online at www.sciencedirect.com
SCIENCE DIRECT®
Journal of Solid State Chemistry 179 (2006) 323–330
JOURNAL OF SOLID STATE CHEMISTRY
www.elsevier.com/locate/jssc

Mechanochemical synthesis and ionic conductivity in the $Gd_2(Sn_{1-y}Zr_y)_2O_7$ ($0 \leqslant y \leqslant 1$) solid solution

K.J. Moreno[a], A.F. Fuentes[a,*], J. García-Barriocanal[b], C. León[b], J. Santamaría[b]

[a]*Cinvestav-Saltillo, Apartado Postal 663, 25000-Saltillo, Coahuila, México*
[b]*GFMC, Departamento de Física Aplicada III, Universidad Complutense de Madrid, 28040 Madrid, Spain*

Received 5 July 2005; received in revised form 22 September 2005; accepted 24 September 2005
Available online 25 October 2005

Abstract

Several compositions within the $Gd_2(Sn_{1-y}Zr_y)_2O_7$ solid solution with a pyrochlore-type of structure, have been prepared at room temperature in a planetary ball mill starting from stoichiometric mixtures of the constituent oxides, SnO_2, ZrO_2 and Gd_2O_3. Phase evolution in the powder mixtures as a function of composition and milling time was followed by X-ray diffraction (XRD) finding out that after 18 h, every mixture consist of a single phase. Mechanically activated chemical reaction takes place after an intial step of particle size refinement and polymorphic transformation of C-Gd_2O_3. We have performed Impedance Spectroscopy measurements to investigate oxygen ion dynamics in the series and conclude that Zr substitution for Sn hardly modifies the importance of ion–ion correlations in the oxygen diffusion process. We also estimate from conductivity measurements the value of the microscopic activation energy needed for independent ion hopping, which is found to be 0.56 ± 0.06 eV, independent of Zr content.
© 2005 Elsevier Inc. All rights reserved.

Keywords: Pyrochlores; Ionic conductivity; Mechanochemical synthesis; Dielectric relaxation; Impedance spectroscopy

1. Introduction

Pyrochlore oxides $A_2B_2O_7$, have received recently much attention because they exhibit a wide variety of important properties of technological interest such as piezoelectricity, ferro- and ferrimagnetism, luminescence, giant magnetoresistance and resistance to radiation damage to mention some [1]. Depending on their chemical composition, the electrical nature of pyrochlore oxides varies from insulators or semiconductors to compounds with high ionic, electronic or mixed conductivity making possible the design of monolithic fuel cells [2]. Thus, while Ca-doped $Gd_2Ti_2O_7$ is a good ionic conductor ($\sigma_i \geqslant 10^{-2}$ S/cm at 1000 °C) [3], $Gd_2Mo_2O_7$ shows at room temperature, a metallic conducting behavior ($\sigma_e \approx 10^{-2}$ S/cm) [4]. From the structural point of view, a fully ordered pyrochlore presents cubic symmetry and belongs to the space group *Fd3m*, being generally referred as a superstructure of the ideal defect fluorite type of structure (space group *Fm3m*), with twice the lattice constant [1]. The ionic conduction mechanism in the pyrochlore structure proceeds mainly via mobile oxygen vacancies migration along the 48*f* sites and depends very much on the degree of structural disorder present in both, the cation and anion sublattices. Such disorder can be induced in some cases by thermal treatment at very high temperatures, by chemical substitution (e.g. as in $Y_2Ti_2O_7$, partially replacing Ti^{+4} for a larger cation such as Zr^{+4}), by ion irradiation or by mechanical milling [5–7]. There are pyrochlores also referred as "defect pyrochlores" which are intrinsically disordered such as $Gd_2Zr_2O_7$ and $Gd_2Sn_2O_7$, and show high oxygen ionic mobility. In particular, ionic conductivity values found at high temperatures for $Gd_2Zr_2O_7$, are comparable to those of yttria stabilized zirconia (YSZ) [8]. We will present in this work a room-temperature route to prepare the $Gd_2(Sn_{1-y}Zr_y)_2O_7$ pyrochlore-type solid solution by dry milling stoichiometric mixtures of the constituent oxides in a planetary ball mill, using a moderate rotating disc speed. We will also analyze oxygen dynamics in the series by using impedance spectroscopy data. Usually prepared by traditional solid-state reaction or by the "liquid mix" technique

*Corresponding author. Fax: +52 844 4389610.
E-mail address: antonio.fernandez@cinvestav.edu.mx (A.F. Fuentes).

0022-4596/$ - see front matter © 2005 Elsevier Inc. All rights reserved.
doi:10.1016/j.jssc.2005.09.036

[9], obtaining pyrochlore oxides require high temperature and long firing cycles. Mechanical milling has been already successfully used in this group for the synthesis of this type of solid solutions [10] and is known to allow preparing metastable materials with a large number of structural defects and vacancies, of relevance in determining ionic mobility in solid electrolytes.

2. Experimental

Several compositions of general formula Gd2$(Sn_{1-y}Zr_y)_2O_7$, were prepared by mechanical milling, starting from stochiometric mixtures of high purity Gd_2O_3 (Aldrich Chem. Inc., 99.9%), SnO_2 (Aldrich Chem. Inc., 99.9%) and ZrO_2 (Aldrich Chem. Inc., 99.99%). Mixed powders were placed in 125 ml zirconia containers with six 20 mm diameter zirconia balls as to keep a balls-to-powder mass ratio of 10:1. Milling was performed in air at room temperature, in a Restch PM/400 planetary ball mill using a rotating disc speed of 350 rpm and reversed rotation every 20 min. The evolution of powder mixtures with composition and milling time, was followed by using X-ray powder diffraction in a Philips X'Pert diffractometer using Ni-filtered Cu$K\alpha$ radiation ($\lambda = 1.5418$ Å) and a step size of 0.01°/s. Impedance studies were carried out from 295 to 900 °C (50 °C steps) on pellets (10 mm diameter and 1 mm thickness) obtained by uniaxially pressing (1500 MPa) the fine milled powders obtained by milling. To increase their mechanical strength and obtain dense samples, pellets were sintered at 1500 °C for 36 h (heating and cooling rate 2 °C/min). Phase purity of sintered samples was analyzed by X-ray diffraction and scanning electron microscopy (SEM) in a Philips XL30 ESEM microscope equipped with an EDAX Inc. energy dispersive X-ray detector for microanalysis, finding no evidence of the presence of second phases. Sample porosities were determined from the accurate measurements of the sample size parameters and weights and by the Archimedes method showing both determinations, good agreement. Ac impedance measurements were carried out in air by using a Solartron 1260 Frequency Response Analyzer over the 100 Hz to 1 MHz frequency range. Electrodes were made by coating opposite faces of the pellets with SPI-Chem™ conductive platinum paint and firing them at 800 °C to eliminate the organic components and harden the Pt residue.

3. Results and discussion

3.1. Synthesis and characterization

Fig. 1a shows an XRD study of the evolution of a Gd_2O_3:SnO_2:ZrO_2 powder mixture (1:0.9:1.1 molar ratio), selected as representative of the series, with milling time. To facilitate the discussion, the characteristic reflections of the starting reagents (cubic Gd_2O_3 (PDF 42-1465), cassiterite SnO_2 (PDF 41-1445) and baddeleyite ZrO_2

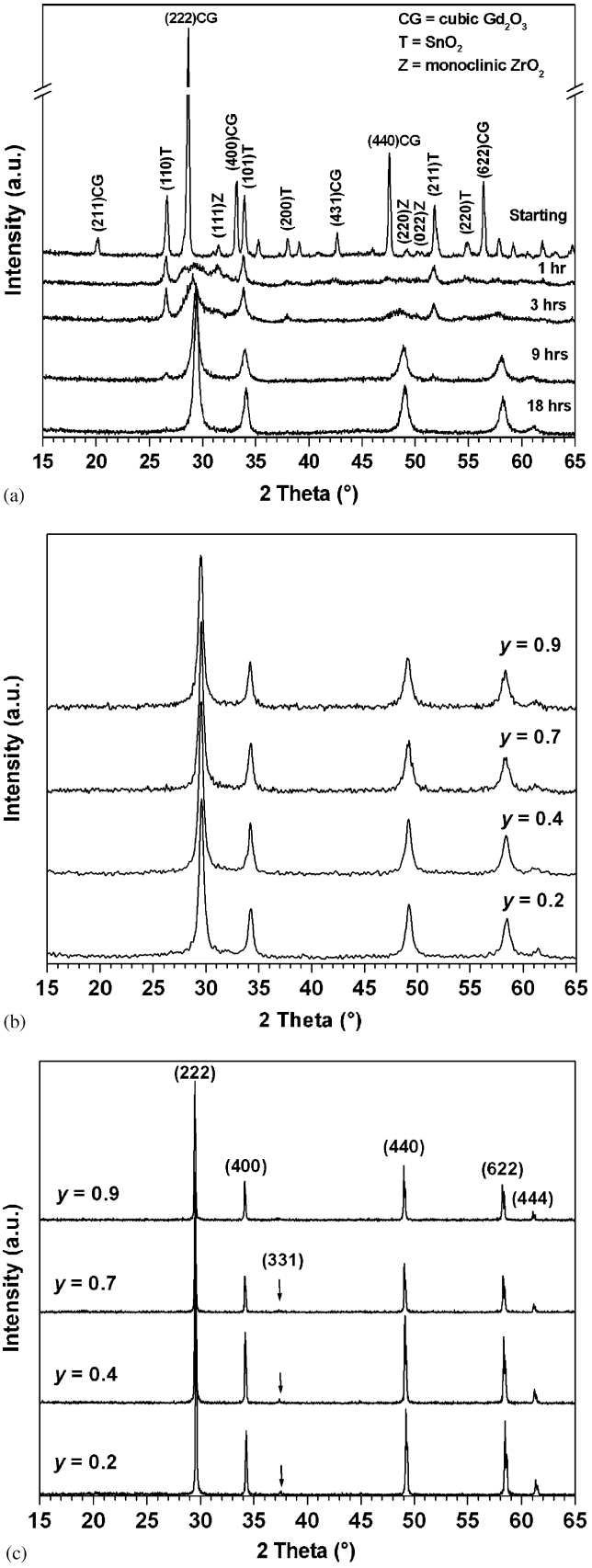

Fig. 1. Evolution of the $Gd_2O_3 + 0.9\ SnO_2 + 1.1\ ZrO_2$ mixture with milling time (a); comparison between the XRD patterns of several compositions within the title solid solution with different Sn/Zr ratio, as taken out of the planetary ball mill (b) and after firing them at high temperatures (c).

(PDF 37-1484)), have been labeled. After the first hour, there is a significant decrease in intensity and broadening of the characteristic diffraction peaks of the starting oxides as a result of the strong decrease of crystallite size and increase in lattice strain taking place during milling. This effect is more significant in Gd_2O_3 which additionally, is known to undergo a polymorphic transformation induced by milling, from the highly symmetric cubic form (C-Gd_2O_3) to the monoclinic B-form as evidenced by the evolution of new reflections in the 29–33° region (2θ). This transformation which is normally temperature driven and is present when the C-form is thermally treated at temperatures above 1200 °C, could also be caused by high-energy milling [11] and it has been found to occur in similar multicomponent systems incorporating Gd_2O_3, prior to the mechanochemically activated chemical reaction taking place [10]. The presence of the characteristic reflections of both, ZrO_2 and SnO_2, is still evident after the first hour. The mechanically activated chemical reaction seems to take place after this initial activation period and after 3 h, the XRD powder pattern contains some reflections which cannot be assigned to any crystalline form of the starting reagents but to a reaction product. Powders milled for 9 h present an XRD pattern which includes some of the main reflections of cassiterite SnO_2 (the {110} and {211} lines at $2\theta = 26.63°$ and 51.83°) and a group of reflections typical of either, an anion deficient fluorite or a pyrochlore type of structure. After 18 h, the most intense line of cassiterite SnO_2 disappears and the only reflections present are those of the reaction product. As mentioned before, fully ordered pyrochlores can be considered as a superstructure of an anion deficient fluorite. Therefore, their characteristic XRD patterns contain a set of strong reflections typical of the underlying fluorite-type average structure plus an additional set of superstructure reflections with decreasing intensity as disorder increases. In fact, anion deficient fluorites can be obtained from fully ordered pyrochlores by disordering both, the cation and anion sublattices. Since both ends of the title solid solution are disordered pyrochlores and samples obtained by mechanical milling are expected to present extensive atomic disorder, XRD patterns of milled samples should be similar to that of an anion deficient fluorite or to that of highly disordered pyrochlores but with weak superstructure reflections. Fig. 1b shows the XRD patterns of four compositions with different Sn^{4+}/Zr^{4+} ratios after milling them for 18 h as described above. The only reflections present are those typical of an anion deficient fluorite type of structure indicating the formation of highly disordered phases. However, the presence of weak lines (e.g. the {331} line at $2\theta \sim 37.5°$) denoting the existence of the pyrochlore superstructure, is evident in the XRD patterns of the same samples fired at 1450 °C (Fig. 1c). Since both, Zr^{4+} and Sn^{4+}, have similar ionic radii (0.72 versus 0.69 Å, both in octahedral coordination) [12], cell size remains relatively unaffected by the partial substitution of one tetravalent cation by the other and XRD patterns are almost identical. Thus, cell parameters calculated by the Rietveld method using the FullProf program [13] and assuming a pyrochlore-type of structure for the whole series (R_A/R_B ratio varies from 1.52 for $Gd_2Sn_2O_7$ to 1.46 for $Gd_2Zr_2O_7$), shows a linear dependence with increasing Zr^{4+} content obeying Vegard's law; values found were included within the 10.471 Å of $Gd_2Sn_2O_7$ to 10.524 Å of $Gd_2Zr_2O_7$ range, similar to that reported by Subramanian et al. for the same compounds, 10.460 and 10.528 Å, respectively [14]. Crystallite size of sintered samples was found to increase with Zr content, from below 400 Å for $Gd_2Sn_2O_7$ to 1041 Å for $Gd_2Zr_2O_7$. Chemical composition of the as-prepared powder samples was analyzed by EDS finding out that the actual composition in every case was close to the nominal one within experimental errors. Measured density values for sintered pellets were above 90% for the whole series, increasing as the Zr content increases. Fig. 2 shows a typical micrograph of a sintered sample obtained for the zirconium rich compositions of the series.

3.2. Electrical measurements

Electrical conductivity in the series has been found to be esentially ionic for samples with compositions $y > 0.5$ and a non-negligible electronic contribution to the total conductivity only appears in the tin-rich samples ($y = 0$ and 0.2) [9]. Although we present experimental data for all the samples analyzed, our analysis of oxygen dynamics have been restricted to those samples samples with negligible electronic conductivity. Therefore, Fig. 3 shows the frequency dependence of the real part of the conductivity and permittivity at several temperatures, for two selected zirconium-rich compositions, $Gd_2(Sn_{0.3}Zr_{0.7})_2O_7$ and $Gd_2(Sn_{0.1}Zr_{0.9})_2O_7$, where conductivity is purely ionic. As Figs. 3a and c show, a Jonscher-type behavior [15] of

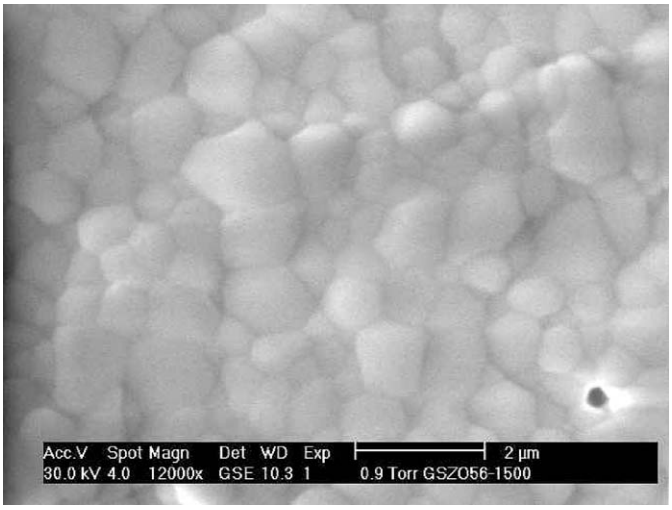

Fig. 2. SEM micrograph of $Gd_2(Sn_{0.3}Zr_{0.7})_2O_7$ powders prepared by mechanical milling and sintered at 1500 °C as described in the experimental section.

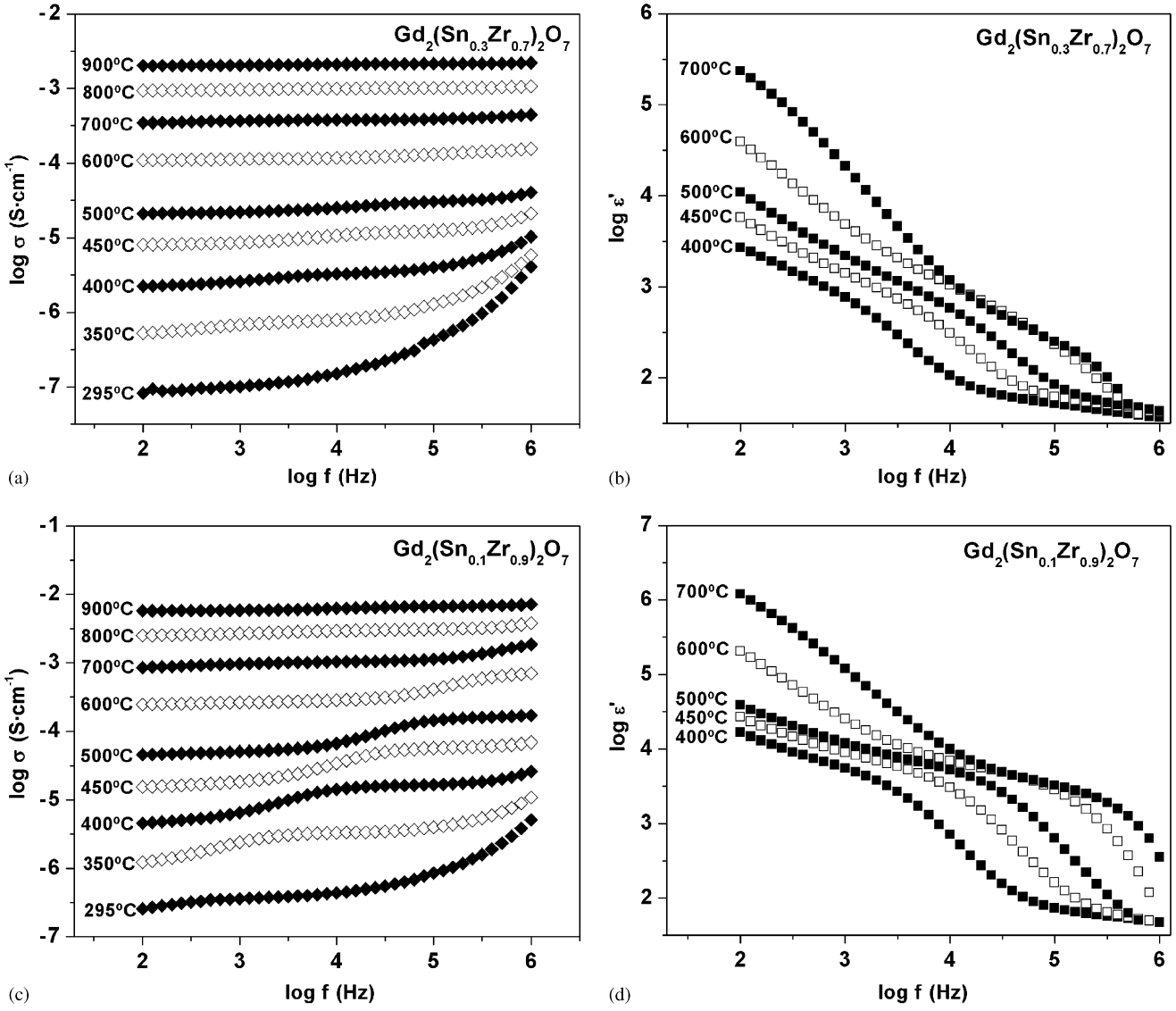

Fig. 3. Evolution of conductivity and permittivity with temperature and frequency for two compositions selected as representatives of the series, $Gd_2(Sn_{0.3}Zr_{0.7})_2O_7$ (a and b) and $Gd_2(Sn_{0.1}Zr_{0.9})_2O_7$ (c and d).

the form:

$$\sigma^*(\omega) = \sigma_{dc}[(1 + (j\omega/\omega_p)^m] \quad (1)$$

is observed. A power-law regime shows up at the lowest temperatures and highest frequencies, while increasing temperature or decreasing frequency leads to a dc conductivity regime with a conductivity value which is frequency independent. In Eq. (1) σ_{dc} is the bulk or dc conductivity value and ω_p is the cross-over frequency between the dc and power-law regimes, and thus the dc conductivity is directly obtained from ac conductivity measurements as the conductivity value in the "plateau" region. Both σ_{dc} and ω_p are found to be thermally activated with about the same activation energy, E_{dc}, of the dc conductivity. The fractional exponent m is related to the degree of ion–ion interactions existing in the ionic hopping process, and lies in the $0 < m < 1$ range. In the case that there are not interactions among ions, i.e. for completely independent and random ion hopping, the exponent m would be 0. The existence of blocking effects is also evident in Figs. 3a and c. Note that there are two frequency independent plateaus separated by a frequency region showing dispersion, evident between 400 and 500 °C, and more clearly in the $Gd_2(Sn_{0.1}Zr_{0.9})_2O_7$ graph. Blocking effects at grain boundaries are responsible for the decrease observed in conductivity as frequency decreases. Therefore, the plateau appearing at lower frequencies is due to the grain boundary contribution to the conductivity while that observed at higher frequencies is related to the bulk contribution. Blocking effects at low frequencies are also clearly evident as plateaus in Figs. 3b and d which show the real part of the dielectric permittivity for both samples, as a function of frequency and temperature. These blocking effects arise at frequencies below 1 MHz at 700 °C and

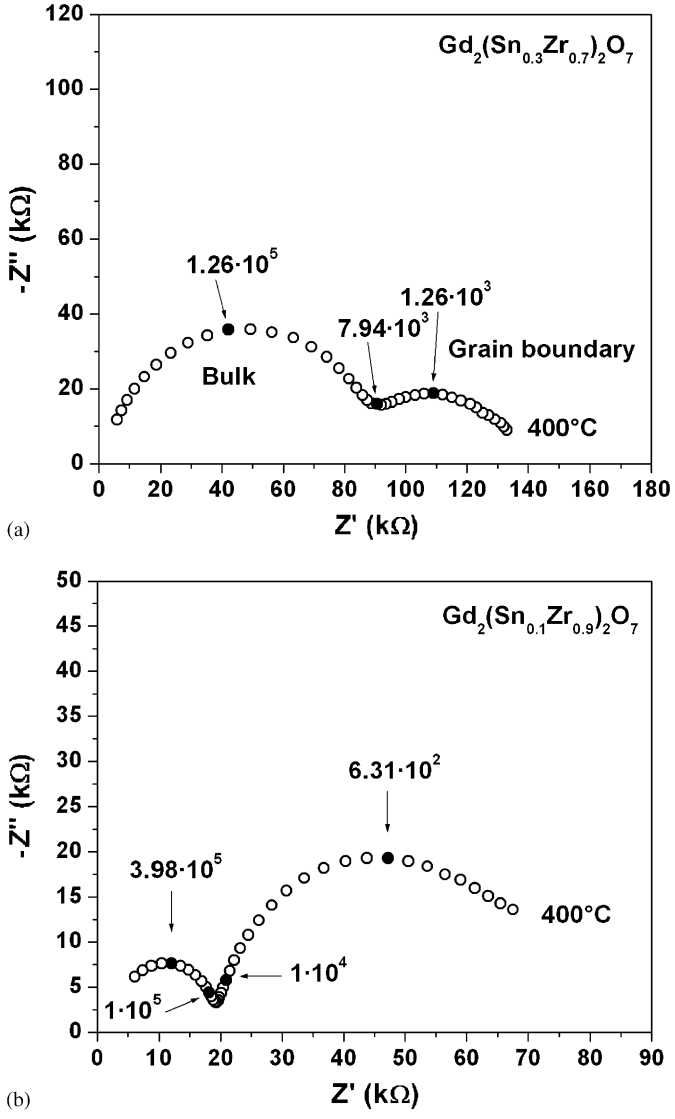

Fig. 4. Complex impedance plots for $Gd_2(Sn_{0.3}Zr_{0.7})_2O_7$ (a) and $Gd_2(Sn_{0.1}Zr_{0.9})_2O_7$ (b) at 400 °C.

confirms that the conductivity at the highest frequencies are dominated by the bulk contribution, even at high temperature. The value of the high-frequency permittivity, $\varepsilon_\infty = 38 \pm 3$, is found to be almost independent of temperature and composition for the whole series. Blocking effects are further confirmed in Figs. 4a and b which present two complex impedance plots for the same compositions of Fig. 3, showing two semicircular arcs with capacitance values typical of bulk (high-frequency arc) and grain boundary contributions (low-frequency arc). Capacitance values found for the high- and low-frequency arcs are 5.13×10^{-11} and 4.23×10^{-9} F/cm for 4a and 5.53×10^{-11} and 1.21×10^{-8} F/cm for 4b, typical of bulk and grain boundary contributions.

Dc conductivity dependence with temperature was analyzed by an Arrhenius equation of the form: $\sigma_{dc}T = \sigma_o \exp(-E_{dc}/k_BT)$, where σ_o is the pre-exponential factor related to the effective number of mobile species and E_{dc} denotes the dc activation energy for the conduction process. Fig. 5a shows such Arrhenius representations for each composition studied in this work, where the lines are fits to the above equation confirming that the process is, in all cases, thermally activated. The activation energy and pre-exponential factor for each composition were calculated from the slope and intercept, respectively, of such linear fits in the Arrhenius plots. The activation energy for the whole series was found to be within the 0.99–1.10 eV interval, relatively unaffected by the change in chemical composition, except for the $Gd_2(Sn_{0.8}Zr_{0.2})_2O_7$ composition, with an activation energy sensibly higher, 1.20 eV.

Fig. 5b presents the evolution of conductivity with zirconium content and temperature for the whole solid solution. After an initial decrease in conductivity for $y = 0.2$, a high increase in conductivity of three orders of magnitude is observed for all temperatures when increasing zirconium content ($y > 0.2$), becoming almost independent of the Zr content for compositions with $y > 0.7$. A similar behavior was described by Yu and Tuller when studying electrical properties of the same solid solution prepared by the "liquid mix" technique [9].

There are in $A_2B_2O_7$ pyrochlores (S.G. *Fd*3*m*) such as $Gd_2(Sn_{1-y}Zr_y)_2O_7$, two available positions for cations and three for anions. Thus, A and B cations will order in alternating rows along the <110> direction and will occupy the 16*c* (000) and 16*d* $(\frac{1}{2}\frac{1}{2}\frac{1}{2})$ positions, respectively. There are three positions available for the oxygen atoms: two, the 48*f* $(x\frac{1}{8}\frac{1}{8})$ and 8*a* $(\frac{1}{8}\frac{1}{8}\frac{1}{8})$ sites, fully occupied and one, the 8*b* $(\frac{3}{8}\frac{3}{8}\frac{3}{8})$ site, nominally empty. These positions present different local atomic environments and while the 48*f* sites are surrounded by two B^{4+} (Sn^{4+} and/or Zr^{4+} in our case) and two A^{3+} cations (Gd^{3+} in our case), the 8*a* site is coordinated by four A^{3+} ions and the 8*b*, by four B^{4+} atoms. Disordered or "*defect*" pyrochlores will present a partially occupied 8*b* site with oxygen atoms from the nearest-neighbor oxygen shell, the 48*f* site. Oxygen atoms in 8*a* will only participate in the occupation of the 8*b* site for highly disordered structures, close to the pyrochlore to fluorite phase boundary. Using computing simulation techniques, van Dijk et al. [16] proposed oxygen Frenkel defects of the type 48*f* vacancy and 8*b* interstitial as the most stable intrinsic defects to be present in $Gd_2Zr_2O_7$ requiring 1.96 eV per defect. In fact, they predicted for pyrochlores an actual defect structure consisting of "split vacancies", a 48*f* vacancy pair in the <110> direction with an interstitial ion in between, a scenario slightly more stable (by 0.2 eV) than a single 48*f* vacancy. A diffusion mechanism consisting of sequential jumps of oxygen atoms along the 48*f* sites, either between (i) nearest neighbor sites (along <100>) and/or (ii) along <110> involving the "split vacancy" structure (next nearest neighbor), was proposed as responsible for the migration of vacancies. In a more recent work, Pirzada et al. examined the 48*f* vacancy configuration for a large number of $A_2B_2O_7$ compounds (A = Lu to La, B = Ti to Pb) concluding that the "split vacancy" configuration

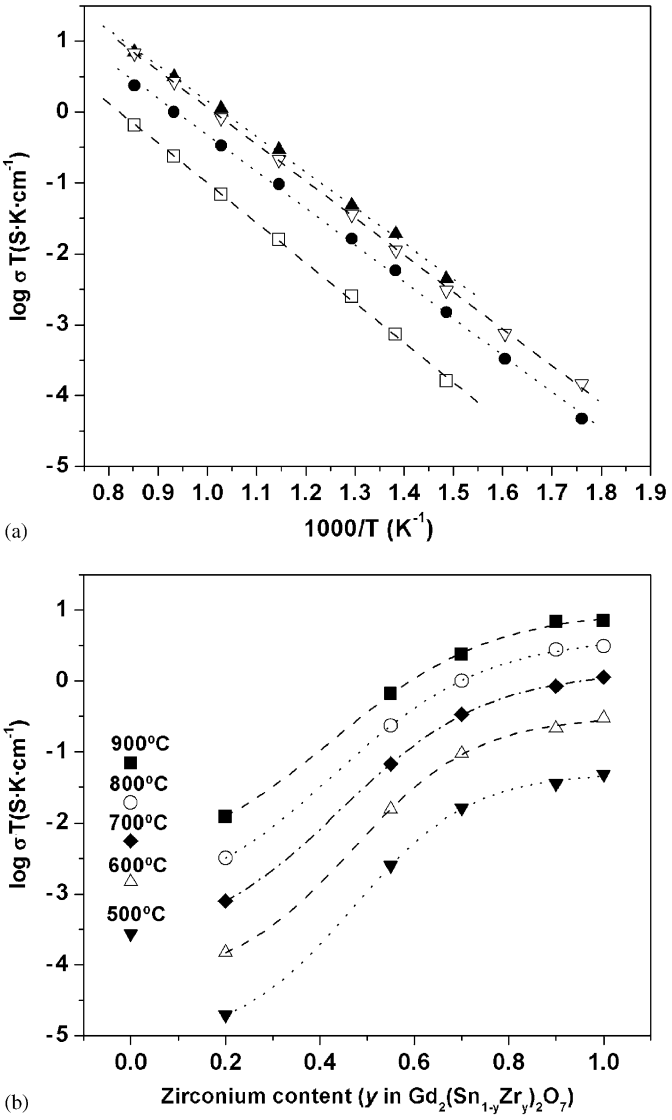

Fig. 5. Arrhenius plots of dc conductivity (a) and conductivity as a function of Zr content and temperature (b) for $Gd_2(Sn_{1-y}Zr_y)_2O_7$ ($0 \leqslant y \leqslant 1$); dotted lines in (b) are only drawn to show trends. For (a), $y = 0.55$ (□), 0.7 (●), 0.9 (▽) and 1 (▲).

proposed by van Dijk et al., becomes more stable with respect to the single vacancy, as the pyrochlore to fluorite phase boundary is approached (when the R_A/R_B ratio comes close to 1), that is, for highly disordered pyrochlores [17]. According to them, for compounds which do not exhibit "split vacancy" formation, all oxygen ion jumps will be along the ⟨100⟩ direction while for those who do, the overall mass transport would be much more complex and not along the ⟨100⟩ direction but on average, along the ⟨111⟩ direction. While their calculations show that the $Gd_2Sn_2O_7$ has no preference for either configuration of vacancies, "split vacancies" will form in $Gd_2Zr_2O_7$. Since the $Gd_2Sn_2O_7$ anion sublattice is highly disordered and the disorder in the series remains relatively unaffected by the Sn^{4+}/Zr^{4+} ratio [9], the increase in oxygen mobility could be due to a change in vacancy configuration as the Zr content increases. Thus, the vacancy migration mechanism in the title solid solution should move from one consisting mainly of a single 48*f* to 48*f* hopping process along the ⟨100⟩ direction for the tin-rich end compositions, to one, for the zirconium-rich end, where the "split vacancy" configuration providing greater geometrical flexibility and longer effective jump distances, would make additional contributions and enhance the ionic mobility. The existence of the "split vacancy" configuration has been experimentally proved by Chen et al. using X-ray photoelectron spectroscopy [18].

Yu and Tuller [9] proposed the increase in oxygen mobility as the tin content decreases to be related with the higher polarizability of the electronic cloud of Zr^{4+} versus Sn^{4+}. Since each 48*f* oxygen position is surrounded by two A^{3+} and two B^{4+} cations, the substitution of Sn^{4+} atoms by the highly polarizable Zr^{4+} atoms should improve oxygen vacancy mobility. Using first principle calculations based on density functional theory, Panero et al. [19] found out that the substantially more covalent ⟨Sn^{4+}–O⟩ bonding in $Y_2Sn_2O_7$ as compared with the ⟨Zr^{4+}–O⟩ bonding in $Y_2Zr_2O_7$, renders a substantially higher Frenkel defect formation energy for the first, much larger than expected taking into account only differences in sizes ($Y_2Sn_2O_7$ is much more resistant to defect formation). In fact, the formation energies calculated for the yttrium tin oxide were almost identical to those found for its similar $Y_2Ti_2O_7$ despite of the large difference in ionic radii between Ti^{4+} and Sn^{4+}.

A good knowledge of oxygen hopping dynamics in solid oxide ion conductors is essential in the search for new insights and understanding of oxygen motion. We present in the following an analysis of the dispersion of the ac conductivity data of these series which is related to the hopping dynamics of mobile ions. As already mentioned above, the power-law regime in the frequency dependence of the real part of the conductivity is the result of the slowing down of the electrical conductivity relaxation process due to cooperative effects among ions in their hopping motion. The same power-law behavior becomes also evident when analyzing the electric modulus formalism, M^*, in the time domain, which is the reciprocal of the permittivity ($M^* = 1/\varepsilon^*$) and physically corresponds to the relaxation of the electric field inside the material when the electric displacement remains constant [20]. Thus, the electric modulus represents the electric field relaxation process and its frequency dependence can be expressed as

$$M^*(\omega) = M_\infty \left[1 - \int (-\mathrm{d}\Phi/\mathrm{d}t)\mathrm{e}^{-\mathrm{j}\omega t}\,\mathrm{d}t\right], \qquad (2)$$

where $\Phi(t)$ is a Kohlraush–Williams–Watts (KWW)-type relaxation function of the form $\Phi(t) = \exp(-(t/\tau_\sigma))^\beta$ with τ_σ a characteristic relaxation time which is also thermally activated and the β exponent an index of the degree of ion–ion correlations in ionic motion ($0 < \beta \leqslant 1$), with $\beta = 1$ for uncorrelated ion hopping. The observation of a non-Debye relaxation behavior characterized by a fractional β

exponent is characteristic of the electric field relaxation in ionic conductors. Different models have been proposed to analyze electrical relaxation data in ionic conductors [21,22], all based on the idea that the hopping event involves many particle (ion–ion) interactions. Both the fractional exponent m that appears in Eq. (1) and the stretching exponent β of the KWW relaxation function appearing in Eq. (2), are thus measurements of the degree of cooperativity in ion hopping dynamics.

Fig. 6a shows the frequency dependence of the imaginary part of the electric modulus between 295 and 600 °C for the composition $Gd_2(Sn_{0.3}Zr_{0.7})_2O_7$ selected as representative of the series. Solid lines are fits to expression (2). Similar fits were obtained for all compositions prepared in this work. As Fig. 6a shows, modulus peaks shift towards low frequencies when the temperature is decreased and only for low temperatures such peaks can be resolved in our frequency window. Fig. 6b presents the frequency dependence of the imaginary part of M^* normalized in order to collapse the peak maxima for some of the compositions prepared in this solid solution. The deviation from a Debye-type behavior is also evident in this figure by the presence of asymmetric peaks, since the slope at the low frequency side of the peaks is always 1 while at the high frequency side is given by $-\beta$. Thus, the different broadening of the peaks for the different compositions corresponds to different β values in the KWW function fit of the peak maxima (Eq. (2)).

An important characteristic of the β exponent is that it relates the macroscopic activation energy for the dc conductivity, E_{dc}, to a microscopic activation energy E_a through the equation $E_a = E_{dc}\beta$ [22]. According to the Coupling Model [22], the microscopic activation energy E_a is the activation energy for independent ion hopping or the energy barrier for oxygen ions to hop into neighboring vacant sites. Since both β and E_{dc} have been obtained from experimental data, we can calculate the energy E_a and get an estimate of the energy barrier for oxygen ions to jump from 48*f* to 48*f* sites in the series. Fig. 7 presents the microscopic activation values (E_a) and those of β found for the title solid solution as a function of Zr content for those samples where conductivity is only due to mobile oxygen ions. Interestingly, the microscopic activation energy was found to be $E_a = 0.56 \pm 0.06$ eV, almost independent of Zr content, which is reasonably expected for the energy barrier for oxygen hopping in the whole solid solution. In a previous work carried out in this group with the similar $Gd_2(Ti_{1-y}Zr_y)_2O_7$ solid solution, it was found that the exponent β decreases from $\beta = 0.85$ to 0.55 by increasing structural disorder, that is, by increasing Zr content: a higher mobile ion concentration enhances mutual interactions and the more disordered structure fosters correlations [23]. However, for the present system $Gd_2(Sn_{1-y}Zr_y)_2O_7$

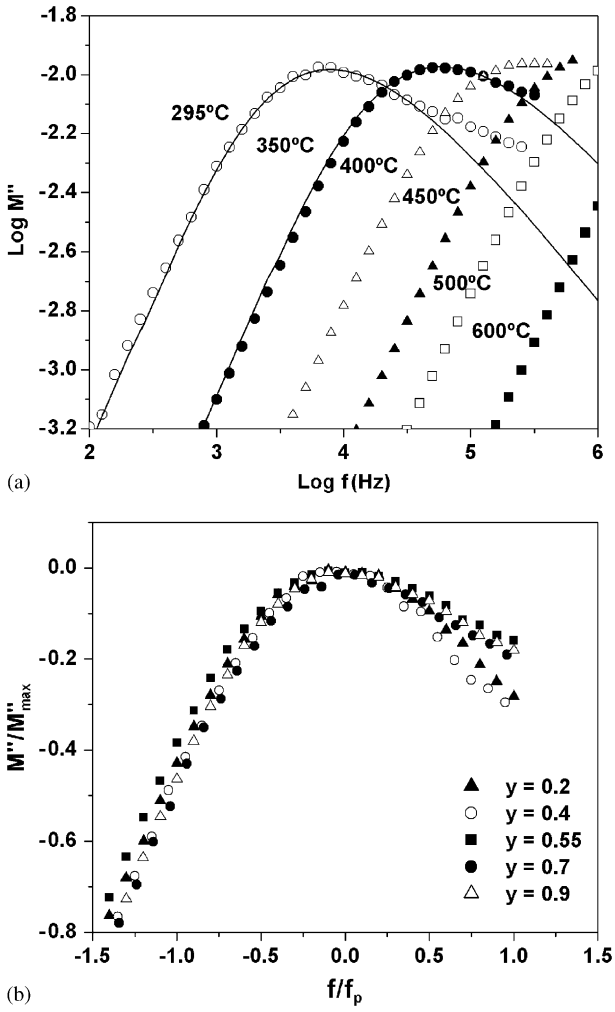

Fig. 6. (a) Frequency dependence of the imaginary part of the electric modulus of $Gd_2(Sn_{0.3}Zr_{0.7})_2O_7$ at selected temperatures. (b) The imaginary part of the electric modulus for different compositions within the title solid solution where experimental data have been shifted horizontally and vertically for clarity.

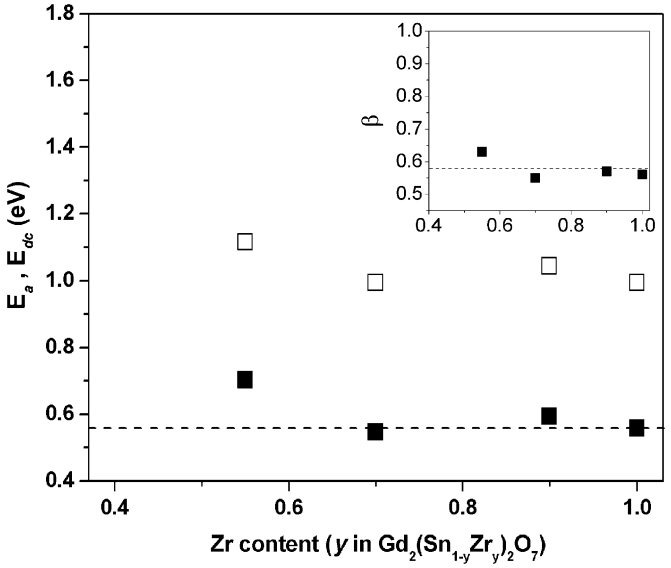

Fig. 7. Activation energies E_{dc} (□) and E_a (■) as a function of Zr content. Inset: Dependence of the exponent β, obtained from fits of peak maxima in the Log M'' versus Log f plots, with Zr content for the series.

where all compositions show a high degree of disorder in the pyrochlore-type structure, we find that the exponent β is essentially independent of the zirconium content and takes a value of about $\beta = 0.58 \pm 0.03$ for all the samples analyzed. This result further confirms that the exponent β, being a measure of ion–ion correlations, is determined by the degree of structural disorder in these samples.

4. Conclusions

Several compositions in the $Gd_2(Sn_{1-y}Zr_y)_2O_7$ solid solution have been successfully prepared at room temperature, by ball milling at a moderate rotating speed, stoichiometric mixtures of high purity constituent oxides (SnO_2, Gd_2O_3 and ZrO_2). The electrical properties of the series were measured as a function of frequency and temperature. The analysis of the ac conductivity data obtained by impedance spectroscopy according to the coupling model allowed us to estimate the energy barrier for oxygen ions to make independent hops into neighboring vacant sites in 0.56 ± 0.06 eV, almost independent of Zr content. In an intrinsically disordered pyrochlore-type solid solution as the one studied in this work, where the degree of disorder is similar for all compositions, the stretching exponent β of the KWW-type relaxation function was found to be 0.58 ± 0.03, essentially independent of the Zr content. Interesting enough, this result differs from that obtained by ourselves when studying the $Gd_2(Ti_{1-y}Zr_y)_2O_7$ solid solution which presents increasing disorder as the Zr content increases, proving therefore that the exponent β value (a measure of ion–ion correlations) is determined by the degree of structural disorder in these samples.

Acknowledgments

This work has been carried out with the financial assistance of CONACYT (SEP-2003-C02-44075).

References

[1] M. Subramanian, G. Aravamudan, G.V. Subba Rao, Prog. Solid State Chem. 15 (1983) 55–143.
[2] H.L. Tuller, in: F. Poulsen, N. Bonanos, S. Linderoth, M. Mogensen, B. Zachau-Chistiansen (Eds.), Proceedings of the 17th Riso International Symposium on Materials Science, Riso National Laboratory, Roskilde, Denmark, 1996, pp. 139–153.
[3] S.A. Kramer, H.L. Tuller, Solid State Ion. 82 (1995) 15–23.
[4] M.A. Subramanian, G. Aravamudam, G.V. Subba Rao, Mater. Res. Bull. 15 (1980) 1401–1408.
[5] P.K. Moon, H.L. Tuller, in: G. Nazri, R.A. Huggins, D.F. Shriver (Eds.), Solid State Ionics, Materials Research Society Proceedings, vol. 135, Mater. Res. Soc. Proc., Pittsburgh, PA, 1989, pp. 149–163.
[6] J. Lian, L. Wang, J. Chen, K. Sun, R.C. Ewing, J.M. Farmer, L.A. Boatner, Acta Mater. 51 (2003) 1493–1502.
[7] A.F. Fuentes, K. Boulahya, M. Maczka, J. Hanuza, U. Amador, Solid State Sci. 7 (2005) 343–353.
[8] A.J. Burggraaf, T. van Dijk, M.J. Verkerk, Solid State Ion. 5 (1981) 519–522.
[9] T.-H. Yu, H.L. Tuller, Solid State Ion. 86–88 (1996) 177–182.
[10] K.J. Moreno, R.S. Rodrigo, A.F. Fuentes, J. Alloys Compds. 390 (2005) 230–235.
[11] D. Michel, L. Mazerolles, P. Berthet, E. Gaffet, Eur. J. Solid State Inorg. Chem. 32 (1995) 673–682.
[12] R.D. Shannon, Acta Crystallogr. A 32 (1976) 751–767.
[13] J. Rodriguez-Carvajal, Physica B 19 (1993) 55–69.
[14] M.A. Subramanian, G. Aravamudan, G.V. Subba Rao, Prog. Solid State Chem. 15 (1983) 55–143.
[15] A.K. Jonscher, Dielectric Relaxation in Solids, Chelsea Dielectrics Press Ltd., London, 1983.
[16] M.P. van Dijk, A.J. Burggraaf, A.N. Cormack, C.R.A. Catlow, Solid State Ion. 17 (1985) 159–167.
[17] M. Pirzada, R.W. Grimes, L. Minervini, J.F. Maguire, K.E. Sickafus, Solid State Ion. 140 (2001) 201–208.
[18] J. Chen, J. Lian, L.M. Wang, R.C. Ewing, R.G. Wang, W. Pan, Phys. Rev. Lett. 88 (2002) 105901.
[19] W.R. Panero, L. Stixrude, R.C. Ewing, Phys. Rev. B 70 (2004) 054110.
[20] P.B. Macedo, C.T. Moynihan, R. Bose, Phys. Chem. Glasses 13 (1972) 171–179.
[21] K. Funke, J. Non-Cryst. Solids 172–174 (1994) 1215–1221.
[22] K.L. Ngai, K.Y. Tsang, Phys. Rev. E 60 (1999) 4511.
[23] K.J. Moreno, G. Mendoza-Suárez, A.F. Fuentes, J. García-Barriocanal, C. León, J. Santamaría, Phys. Rev. B. 71 (2005) 132301.